Histol Histopathol (2013) 28: 1073-1087
DOI: 10.14670/HH-28.1073

http://www.hh.um.es

Histology and Histopathology
Cellular and Molecular Biology

The peculiar apoptotic behavior of skeletal muscle cells

Sara Salucci[1], Sabrina Burattini[1], Valentina Baldassarri[1], Michela Battistelli[1], Barbara Canonico[1], Aurelio Valmori[2], Stefano Papa[1] and Elisabetta Falcieri[1,2]

[1]Department of Earth, Life and Environmental Sciences, University of Urbino "Carlo Bo", Urbino, Italy and
[2]Institute of Molecular Genetics, IGM-CNR, Rizzoli Orthopaedic Institute, Bologna, Italy

Summary. Apoptosis plays an active role in maintaining skeletal muscle homeostasis. Its deregulation is involved in several skeletal muscle disorders such as dystrophies, myopathies, disuse and sarcopenia.

The aim of this work was to study *in vitro* the apoptotic behavior induced by etoposide, staurosporine and hydrogen peroxide in the C2C12 skeletal muscle cell line, comparing myoblast vs myotube sensitivity, investigated by means of morphological and cytofluorimetric analyses.

Myotubes appeared more resistant than myoblasts to apoptotic induction. In myoblasts treated with etoposide, nuclei with chromatin condensation were observed, in the presence of a diffuse DNA fragmentation, as shown by confocal microscopy. The latter also appeared in myotubes, where apoptotic and normal nuclei coexisted inside the same syncytium. After staurosporine treatment, myobalsts evidenced late apoptotic features and a high number of TUNEL-positive nuclei. Secondary necrosis appeared in myotubes, where myonuclei with cleaved DNA again coexisted with normal myonuclei. After H_2O_2 exposure, myotubes, differently from myoblasts, showed a poor sensitivity to cell death. Intriguingly, autophagic granules appeared abundantly in myotubes after each treatment. In myotubes, mitochondria were better preserved than in myoblasts since those which were damaged were probably degraded through autophagic processes.

These findings demonstrate a scarce sensitivity of myotubes to apoptotic stimuli due to acquisition of an apoptosis-resistant phenotype during differentiation. The presence of nuclear-dependent "territorial" death domains in the syncytium could explain a slower death of myotubes compared to mononucleated cells. In addition, autophagy could preserve and protect muscle cell integrity against chemical stimuli, making C2C12 cells, in particular myotubes, more resistant to apoptosis induction.

Key words: Myobasts, Myotubes, Chemical triggers, Apoptosis, Autophagy

Offprint requests to: Prof. Elisabetta Falcieri, Department of Earth, Life and Environmental Sciences, Scientific Campus "Enrico Mattei", Via Ca' le Suore 2, 61029 Urbino (PU), Italy. e-mail: elisabetta.falcieri@uniurb.it

Introduction

In skeletal muscle tissue, apoptosis has an important role in muscle mass development and differentiation (Ferreira et al., 2008; Adhihetty et al., 2009).

Evidence of apoptotic cell death can be found in various skeletal muscle disorders such as muscular dystrophies, mitochondrial myopathies or muscle denervation (Twes, 2003). In all these situations, the high expression of bax, bcl-2 and caspases indicates that under pathological conditions, muscle fibers are capable of mitochondria-mediated events which can lead to apoptosis.

Mitochondria play a central role in apoptosis, especially within skeletal muscle, and are the key players in myocyte loss during aging and other atrophic conditions (Jeong and Seol, 2008; Siu and Alway, 2009; Marzetti et al., 2010). Oxidative damage, impaired respiration and energy production as well as altered mitochondrial turnover have been proposed as potential triggers of the apoptotic signaling. In addition, it is known that among the molecular pathways underlying muscle atrophy, oxidative stress and chronic inflammation may well contribute to muscle wasting correlated to apoptosis and proteolysis activation (Andrianjafiniony et al., 2010).

In our previous study, we demonstrated the apoptotic response of myoblasts exposed to etoposide, staurosporine and hydrogen peroxide (H_2O_2), which are cell death inducers having different mechanisms of action (Salucci et al., 2010). As reported by several authors (Wei et al., 2010; Chen et al., 2011; Liu et al.,

2011; Xiao et al., 2011; Zhang et al., 2011), these chemicals prevalently trigger apoptosis, at least in hematopoietic models, through a mitochondrial pathway.

The aim of the current work is to compare the apoptotic behavior in skeletal muscle, at the undifferentiated (myoblasts) and differentiated (myotubes) stage. The latter condition represents a particular experimental model, being syncytia multinucleated, in which individual nuclei have been reported to control definite muscle fiber segments (Adhihetty et al., 2009).

Inverted (IM), Electron (TEM and SEM) and Confocal Laser Scanning Microscopy (CLSM) as well as Flow Cytometry (FC) were used to investigate different aspects of cell death. In particular, IM permits the monitoring of cell viability, EM permits the identification of nuclear, cytoplasmic and surface apoptotic changes, and CLSM identifies the DNA fragmentation by means of TUNEL reaction. FC quantifies cell parameters providing cell death rate, data on possible double strand DNA cleavage (hypodiploid peak), and general DNA content evaluation before and after chemical treatments.

Materials and Methods

Cell culture

Mouse C2C12 myoblasts, a murine model derived from satellite cells were grown, in flasks or on coverslips in dishes, in the presence of DMEM supplemented with 10% heat-inactivated fetal bovine serum and 2 mM glutamine. After achieving monolayer confluence, the serum was reduced to 1% to induce myogenic differentiation. The cells were maintained in a 5% CO_2 atmosphere at 37°C. The myotubes were then analysed seven days after the induction of differentiation (D'Emilio et al., 2010).

U937 human myelomonocytic lymphoma cell line was grown as reported by Luchetti et al. (2006) and used as a model of classical apoptosis.

Apoptosis induction

Apoptosis was induced by adding 25 μM etoposide, 0.25 μM staurosporine and 500 μM H_2O_2 to culture media for 22 hours. The concentrations of the chemicals were chosen on the basis of our previous work, in which various doses and times were analysed (Salucci et al., 2010).

The cell behavior of control and treated samples was monitored by means of a TE 2000-S Nikon inverted microscope (IM), equipped with a digital Nikon DN100 system.

Transmission Electron Microscopy (TEM)

Myoblasts and myotubes, growing adherent to flasks, were washed and immediately fixed "in situ" with 2.5% glutaraldeyde in 0.1M phosphate buffer for 15 minutes and then gently scraped and centrifuged at 1200 rpm. The pellets were fixed in 2.5% glutaraldehyde for an additional 30 minutes.

U937 cells were processed as previously reported (Burattini et al., 2009).

All the specimens were post-fixed in 1% OsO_4 for 1 hour, alcohol dehydrated and embedded in araldite (Salucci et al., 2010). Thin sections were stained with uranyl acetate and lead citrate and analysed with a Philips CM10 transmission electron microscope.

Scanning Electron Microscopy (SEM)

Control and treated myoblasts and myotubes were directly processed on coverslips in Petri dishes. After careful washing with 0.1M phosphate buffer, monolayers were fixed with 2.5% glutaraldehyde in the same buffer for 1 hour.

U937 cells were cultured and treated in flask and, after washing in 0.1M phosphate buffer, they were fixed in suspension with 2.5% glutaraldehyde in the same buffer for 1hour. Successively, they were deposited on poly-L-lysine-coated coverslips overnight at 4°C. All the specimens were post-fixed with 1% OsO_4 in 0.1M phosphate buffer for 1 hour. After alcohol dehydration, they were critical point dried, gold sputtered, and observed with a Philips 515 scanning electron microscope (D'Emilio et al., 2010).

TUNEL

Control and treated muscle cells, directly processed on coverslips in Petri dishes, were washed and fixed with 4% paraformaldehyde in PBS pH 7.4 for 30 min, rinsed with PBS and permeabilized with a mixture 2:1 of ethanol and acetic acid for 5 min at -20°C. For the TUNEL technique, all reagents were part of the Apoptag Plus, (D.B.A.) and procedures were carried out according to the manufacturer's instructions. Cells were treated with TdT buffer for 10 minutes at room temperature and incubated with the reaction buffer containing the TdT enzyme for 1 hour at 37°C in a humidified chamber. The reaction was blocked by the stop buffer for 10 minutes. Cells were incubated with a FITC-conjugated anti-digoxigenin antibody for 30 minutes at room temperature. Lastly, slides were mounted with an antifading medium (Zamai et al., 2004; Burattini et al., 2009). Specimens were observed with a Leica TCS-SP5 connected to a DMI 6000 CS Inverted Microscope (Leica Microsystems CMS GmbH; excitation was at 488 nm and emission signals were detected at 517 nm).

Flow Cytometry (FC)

Each cell pellet was fixed with 70% cold ethanol and kept at -20°C for at least 1 day. Cells were washed twice with PBS and pellets were re-suspended in a citrate

buffer containing 20 μg/ml propidium iodide (PI) and 100 μg/ml RNAse.

Undifferentiated and differentiated C2C12 cells were additionally treated with 0.2% TRITON X-100 and re-suspended 2-3 times using small pipette tips to increase cellular disaggregation, particularly for the longest myotubes. Our group (D'Emilio et al., 2010) and many other authors (Wang et al., 1997; Zhang and Cox, 1998; Ghosh and Barry, 2005; Govindaraju et al., 2006; Munoz et al., 2010) have performed FC on differentiated muscle cells, not only to evaluate DNA content but also to analyse surface staining and cell functions.

The samples were kept at 37°C in the dark for at least 30 min and analysed, for cell cycle profile and other cellular parameters, by means of a FACScalibur flow cytometer equipped with two lasers (Canonico et al., 2010). In our entire protocol, we were careful to minimize the loss of cells during harvesting and washing. The data were then acquired and analysed by the CellQuestTM flow cytometry software (Becton Dickinson, San Jose, CA).

To label fresh cells, we added the different fluorochrome in the appropriate volume to each of the experimental conditions. The cardiolipin-sensitive probe 10-nonyl acridine orange (NAO) was used to monitor mitochondrial lipid changes (Luchetti et al., 2007). We incubated cells with NAO to a final concentration of 100 nM for 20 min at 37° C. Green (FL1) fluorescence emission illuminated with blue (488 nm) excitation light was measured by FC.

The pH-sensitive dye Acridine Orange (AO) can be used to detect Acidic Vacuolar Organelle (AVO) formation. It can enter acidic compartments, such as lysosomes and autolysosomes, where it becomes protonated and sequestered (Traganos and Darzynkiewicz, 1994). At low pH, AO emits red fluorescence with an intensity proportional to the degree of acidity and/or to the acidic compartment volume. Therefore, AVO formation in AO-stained cells can be measured by flow cytometry or, alternatively, can be observed under a fluorescence microscope. Cells were stained with 75ng/ml Acridine Orange for 15 min at 37°C.

SYBR GREEN I is able to stain nucleic acids with a higher quantum yield when it binds to DNA than when it binds to RNA (Lebaron et al., 2001). The staining with this fluorochrome was performed with a final dilution of 1:10000.

Results

IM, TEM, SEM and CLSM analyses

After IM observation, the control cells (Fig. 1) revealed a good viability. A star or fusiform shape was observed in myoblasts (Fig. 1A), which appeared scattered throughout the flask bottom. Myotubes were confluent, very long, and multinucleated (Fig. 1B). TEM confirmed IM observations and allowed a more precise characterization of the nuclear behavior. Control myoblasts (Fig. 1C) usually showed a central nucleus with diffuse chromatin and numerous nucleoli. Several nuclei (up to 200) were observed in the myotubes (Fig. 1D). These were centrally placed and had an irregular profile compared to that of the myoblasts. A well preserved morphology of cytoplasm and organelles was also detected in all cell types at TEM. In addition, the TUNEL reaction, observed at confocal microscopy, was totally negative for both models (Fg. 1E,F).

Ultrastructural analyses evidenced that all treatments generated diffuse cell damage.

After etoposide treatment (Fig. 2), some myoblasts appeared detached, rounded and blebbed at IM (Fig. 2A). The myotubes (Fig. 2B) presented only an apparent nuclear disorganization. After TEM observations, the myoblasts displayed initial chromatin margination and condensation (Fig. 2C). These features were also observed in differentiated cells that revealed a peculiar behavior: within the same myotube, normal nuclei coexisted with apoptotic ones (Fig. 2D). In addition, autophagic vacuoles appeared (Fig. 2D) at the periphery of syncytia. So at TEM, the myonuclei displayed a morphological chromatin rearrangement (condensation and margination) that were similar, if not identical, to that of nuclei undergoing classical apoptosis (Fig. 2E).

The TUNEL reaction observed at confocal microscopy evidenced several nuclei with DNA fragmentation, both in myoblasts (fig. 2F) and myotubes (fig. 2G). The latter presented TUNEL negative and positive myonuclei in the same syncytium (Fig. 2G).

After staurosporine treatment (Fig. 3), C2C12 cell detachment was observed at IM, showing rounding and dying myoblasts (Fig. 3A) as well as strongly modified, particularly thin, myotubes (Fig. 3B). TEM showed a conspicuous secondary necrosis rate in both cell types. A peculiar behavior of chromatin, which appeared organized in dense ring-shaped nuclear patches in both myoblasts (Fig. 3C) and myotubes (Fig. 3D, E), was revealed to be similar to the classic behavior detected in U937 cells (Fig. 3G). Only a few myotubes conserved an intact structure with normal nuclei, but their cytoplasm presented a diffuse vacuolization identified by TEM to be autophagic vacuoles (Fig. 3F). In addition, in myoblasts (Fig. 3H) a diffuse and intense TUNEL positivity appeared, and to a lesser extent in myotubes (fig. 3I) where labeled and normal myonuclei were observed in the same cell.

Membrane blebbing (Fig. 4), absent in the control condition (Fig. 4A-C), was detected by SEM, choosing staurosporine treatment as the representative condition. In the C2C12 cell line, smaller and more numerous blebs could be observed along the surface (Fig. 4D, E), while the blebs appeared as large membrane protrusions in the classical apoptotic model (Fig. 4F).

General cell damage was evidenced after H_2O_2 treatment (Fig. 5). Some myoblasts appeared rounded and detached at IM observation (Fig. 5A), while others were apparently well preserved. Myoblasts with

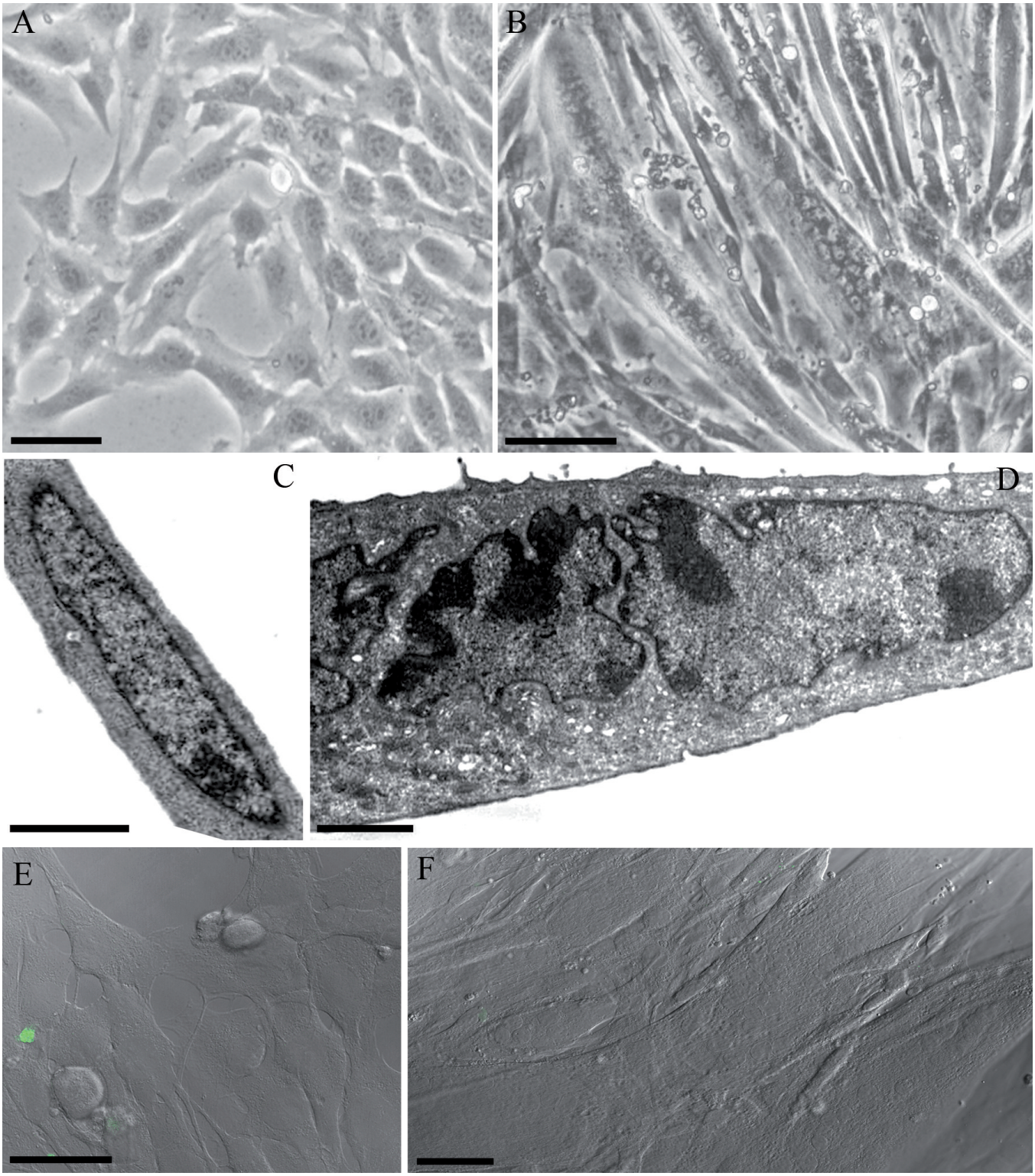

Fig. 1. Control cells seen at IM **(A, B)**, TEM **(C, D)** and CLSM **(E, F)**. C2C12 myoblasts **(A, C, E)** present a star shape or a fusiform appearance. Myotubes **(B, D, F)** show a tubular shape and numerous nuclei. The TUNEL reaction appears negative for both cell types **(E, F)**. Scale bars: A, E, F, 10 μm; B, 20 μm; C, 1 μm; D, 2 μm.

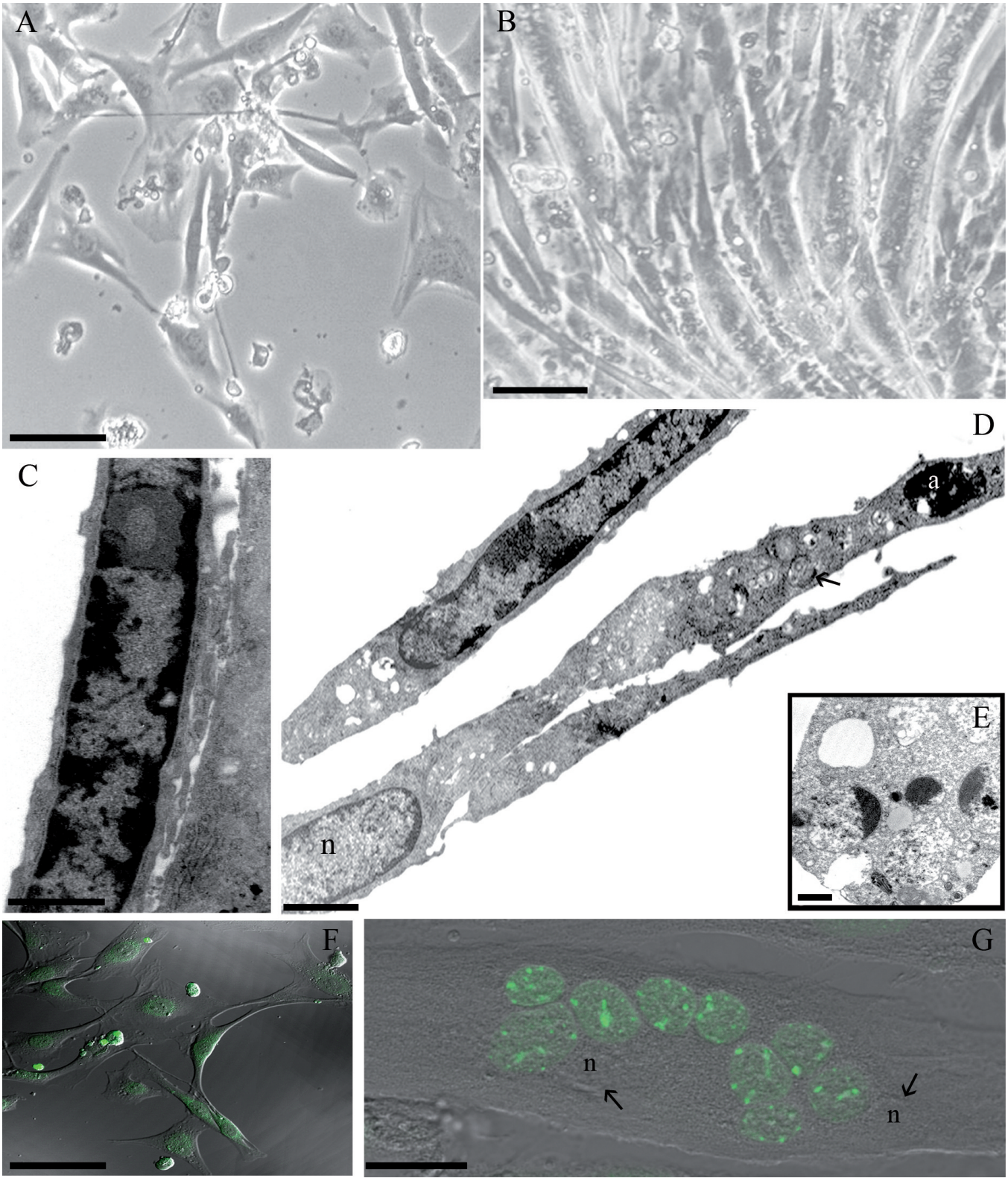

Fig. 2. Cells after etoposide treatment at IM **(A, B)**, TEM **(C, D, E)** and CLSM **(F, G).** A few myoblasts appear to be rounded and blebbed **(A)**. A cell with chromatin margination can be observed **(C)**. Myotubes present general damage at IM **(B)**. In particular, in a single cell **(D)**, apoptotic nuclei (a) coexist with normal nuclei (n) in the presence of a diffuse cytoplasmic vacuolization and autophagic organelles (arrow). Classical apoptotic features appear in U937 cells **(E)**. Diffuse TUNEL labeled nuclei can be observed in both cell types **(F, G)**. In particular, in myotubes **(G)** TUNEL-positive myonuclei appear in the presence of normal nuclei (n, arrows). Scale bars: A, B, F, G, 20 μm; C, D, E, 1 μm.

chromatin condensation (fig. 5C), similar to that detected in U937 cells (Fig. 5F) were observed at TEM. In myotubes, the massive damage evidenced at IM (Fig. 5B) corresponded to a diffuse secondary necrotic cell death (Fig. 5D). Both undifferentiated and differentiated cells exposed to oxidative damage presented a number of autophagic vacuoles (Fig. 5C,E). At confocal microscopy, TUNEL-positive myonuclei were observed more diffusely in myoblasts (Fig. 5G) and, in a lesser number, in myotubes (Fig. 5H).

In C2C12 undergoing all experimental conditions, autophagic vacuoles (fig. 6) were observed, being more diffuse in myotubes, where they contained mitochondria (Fig. 6A B), nuclear material, free ribosomes and membranes (Fig. 6C). On the other hand, in myoblasts they appeared as initial formations (Fig. 6D), probably resulting from mitochondrial degeneration, and were located in proximity of the endoplasmic reticulum.

FC analysis

FC revealed good cell viability conditions in each

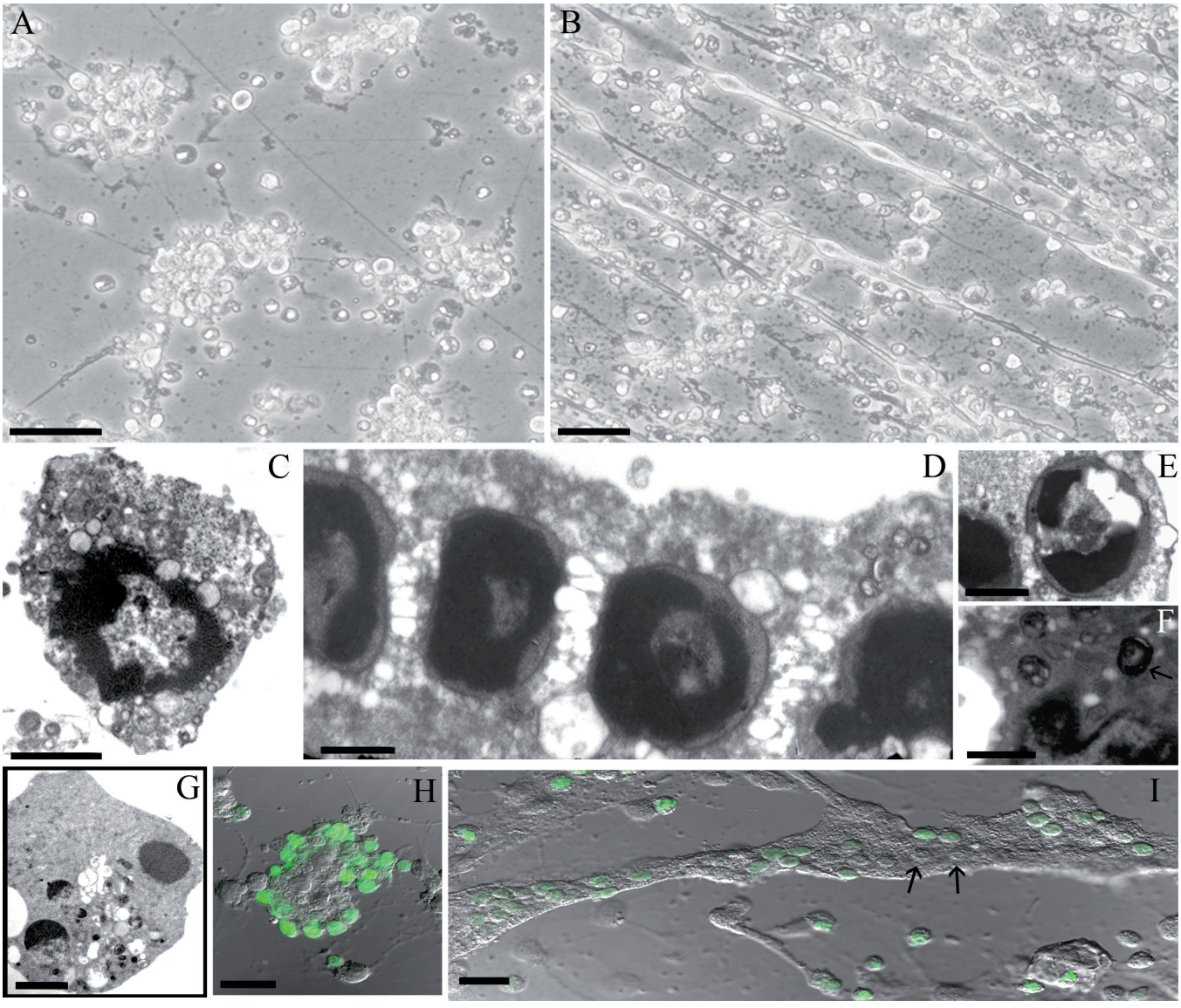

Fig. 3. Cells after staurosporine exposure at IM **(A, B),** TEM **(C, D, E, F, G)** and CLSM **(H, I).** Myoblasts, rounding, detached from the underlying substrate **(A)** and undergoing secondary necrosis **(C)**, appear. The myotubes are mostly dead and, if attached to the substrate, have a thinner shape and damaged nuclei **(B)**. Diffuse secondary necrosis and cells with condensed, ring-shaped chromatin appear **(D, E)**. Autophagic vacuoles can be detected (**F**, arrows). Late apoptotic events can be observed in U937 cells **(G)**. Myoblasts **(H)** show a diffuse and intense DNA fragmentation after TUNEL reaction. In some myotubes **(I)** DNA cleavage appears in the presence of TUNEL-negative nuclei (arrows) in the same syncytium. Scale bars: A, B, 40 μm; C, D, E, G, 2 μm; F, 1 μm; H, I, 20 μm.

control sample (myoblasts and myotubes) Furthermore, forward scatter (FSC) vs side scatter (SSC), is able to visualize the differences in the dot-plot area of myoblasts vs myotubes, also confirmed by 3D isometric display (Fig. 7).

Samples were acquired as ethanol fixed cells (DNA content by PI labelling) and as fresh cells (NAO, AO, SYBR GREEN tests).

DNA content analysis

The DNA histogram pattern was determined by plotting the intensity of PI staining, which reflects the DNA content in each cell, as a function of cell number. The evidence of a clear sub-G1 cell population reveals the presence of apoptotic cells. This typical feature was not observed in both undifferentiated and differentiated C2C12 cells in which a more peculiar DNA content distribution appeared. Fig. 8 shows etoposide to be the only chemical trigger able to induce cell death, at least in terms of small DNA cleavage in C2C12 myotubes.

NAO fluorescence detection

Cytometric analyses revealed the effect of cardiolipin peroxidation on both myoblasts and myotubes, showing a clear mitochondria impairment in undifferentiated C2C12 cells. In fact, frequencies of events characterized by normal cardiolipin (Fig. 9) are lowered by 35% in etoposide-treated myoblasts, by 38% in staurosporine-treated myoblasts and by approximately 40% for H_2O_2-treated cells, indicating the involvement of the mitochondrial pathway and contemporarily the presence of a certain degree of apoptotic death. Furthermore, taking into account Mean Fluorescence Intensity (MFI) values for NAO labelling, we could identify a more intense peroxidation at the single cell level for the staurosporine treatment (MFI: 274 for control cells vs 350). On the contrary, in differentiated C_2C1_2 cells, NAO labelling gave almost the same frequencies as control cells, with the exclusion of H_2O_2 treated cells (10% less than control).

AO fluorescence detection

Lysosomal stability analysis was performed by following the uptake of the weak base Acridine Orange (AO; Sigma), able to trace the organelle acidic compartment. Our data were split into percentages of positivity and MFI values (Fig. 10). Coupling these findings, we can envision this scenario: in myoblasts (Fig. 10E) all treatments provided a high number of events with decreased AO red fluorescence, suggesting a disassembly and/or damage of this cell compartment (lysosome, autophagolysosomes), particularly evident after etoposide and H_2O_2 administration. Intriguingly, MFI (Fig. 10G) data related to the red cell positive fraction revealed values close to control samples for etoposide and values 3-fold higher in staurosporine and H_2O_2 treated cells. Such behavior could be explained by an indirect and subordinate involvement of lysosomes and autophagolysosomes for etoposide-induced cell

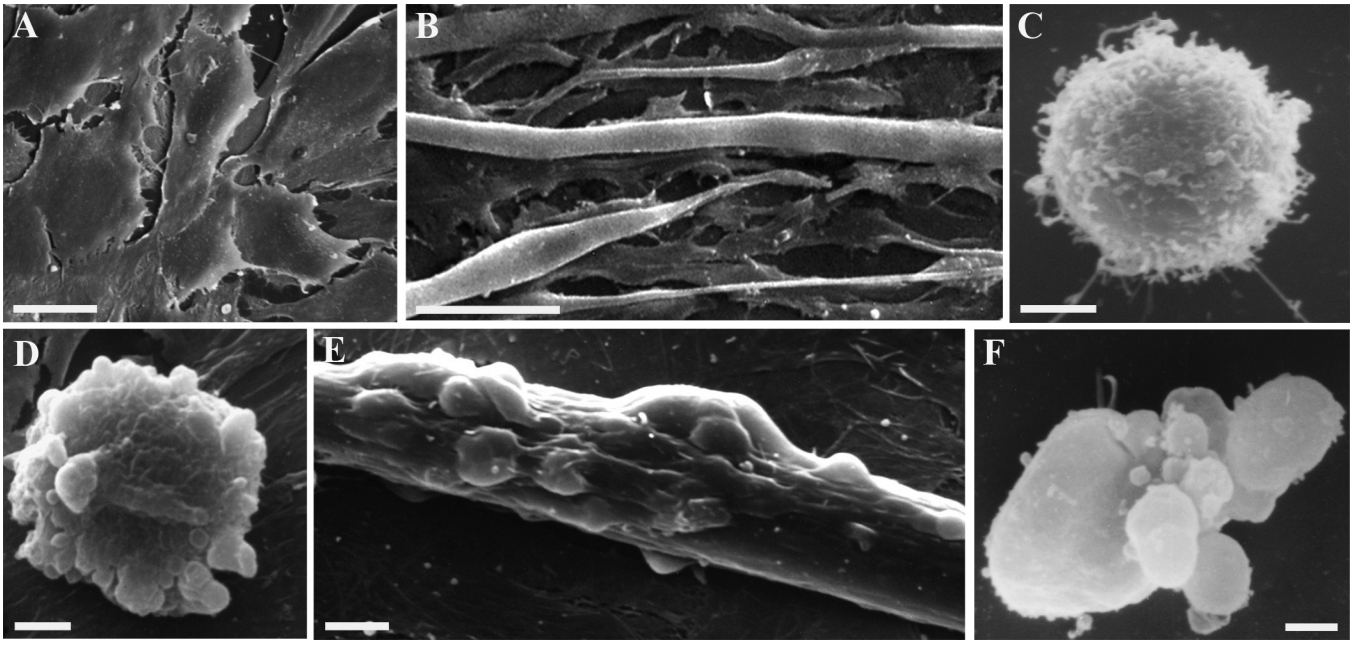

Fig. 4. C2C12 and U937 cells observed at SEM after staurosporine treatment. Control myoblasts **(A)** myotubes **(B)** and U937 cells **(C).** Small blebs can be observed on C2C12 myoblast and myotube surfaces **(D, E)** while in U937 treated cell, large blebs appear **(F)**. Scale bars: A, 20 μm; B, 40 μm; C, D, F, 2 μm; E, 5 μm.

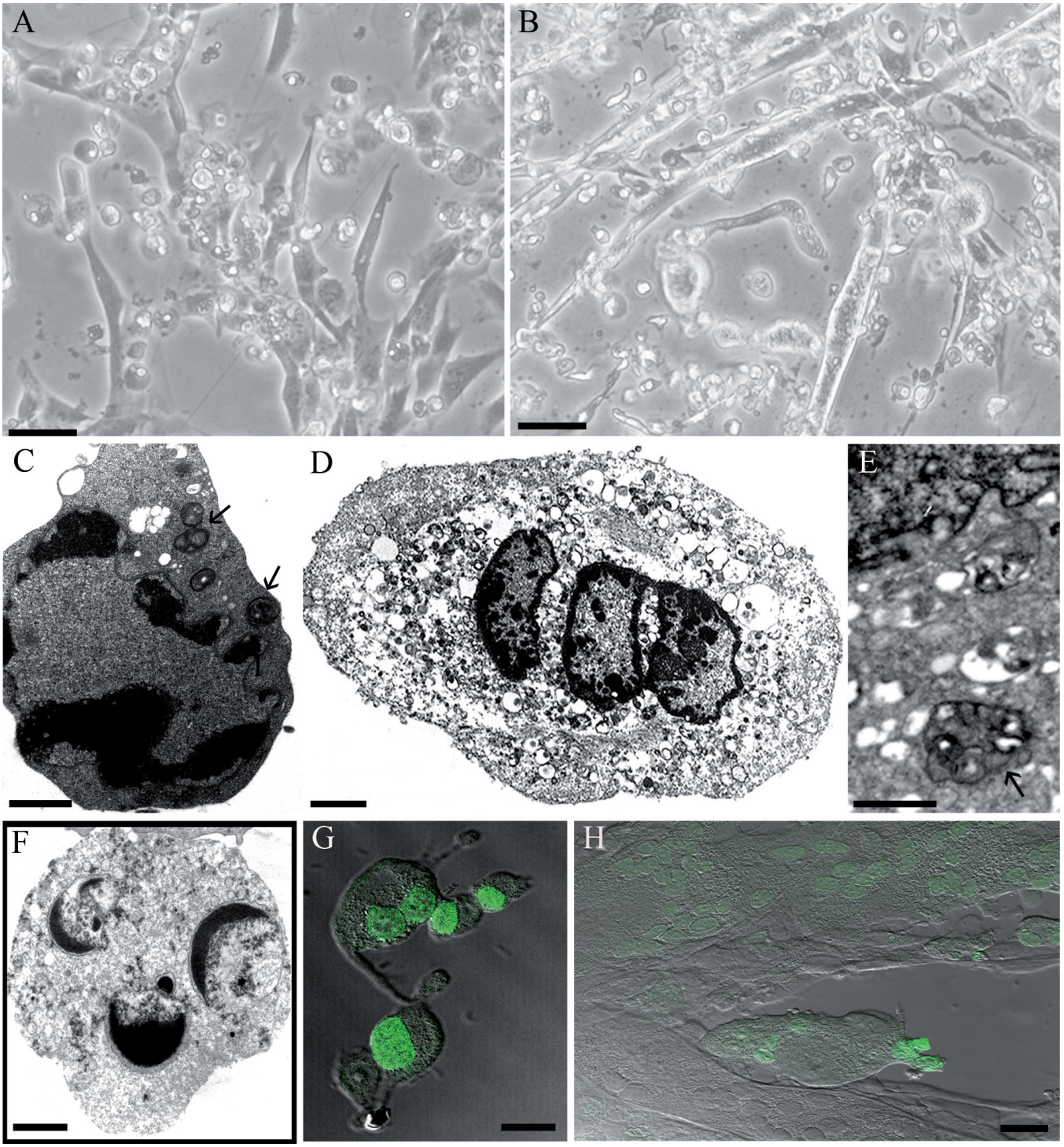

Fig. 5. Cells after H_2O_2 treatment observed at IM **(A, B)**, TEM **(C, D, E, F)** and CLSM **(G, H)**. The C2C12 cells present diffuse cell damage with rounded myoblasts **(A)** and slim myotubes **(B)**. Myoblasts **(C)** display chromatin condensation and cytoplasm vacuolization. In the myotubes **(D)** secondary necrosis can be detected. Moreover, autophagic vacuoles appear in both conditions (**D**, **E**, arrows). Micronuclei appear in U937 cells **(F)**. TUNEL reaction positivity can be observed in myoblasts **(G)** and, with lesser intensity, in myotubes **(H)**. Scale bars: A, B, 20 μm; C, 1 μm; D bar 5 μm; E, 0.5 μm; F, 2 μm; G, 10 μm; H, 25 μm.

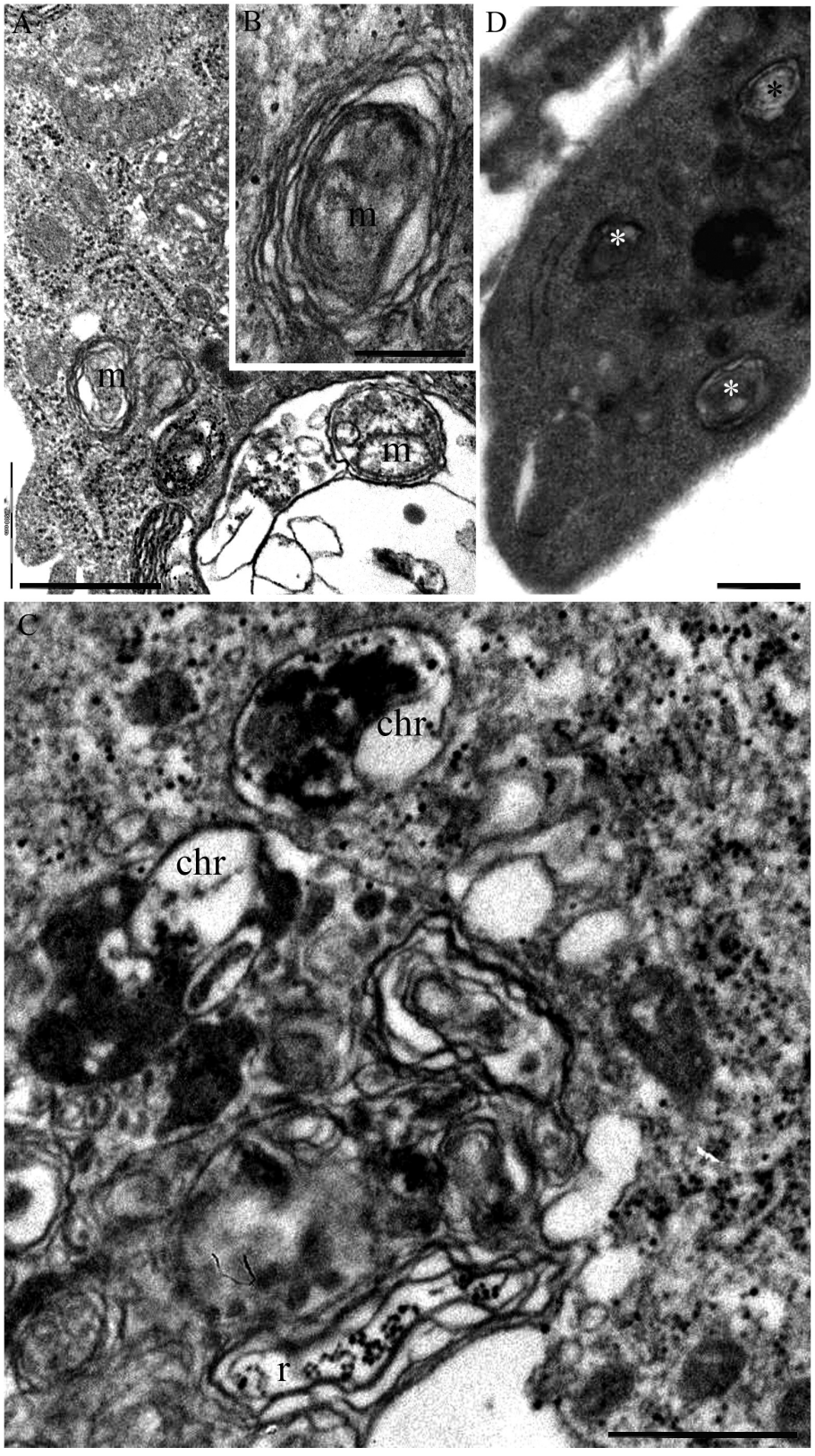

Fig. 6. Autophagy. Swollen and degenerated mitochondria (m), condensed chromatin (chr) inclusions, free ribosomes (r) and membranes can be observed inside autophagic vacuoles in myotubes exposed to H_2O_2 **(A)** or staurosporine (**B, C**). Smaller and initial autophagic organelles (*) appear in myoblasts treated with H_2O_2 **(D)**. Scale bars: A, C, D, 500 nm; B; 250 nm.

death, whereas for staurosporine and H_2O_2, mechanisms of cell death may pass directly to autophagy enhancement. In myotubes (fig. 10F), events with decreased AO red fluorescence are almost absent, highlighting the general stability of acidic organelles in this differentiated stage of C2C12 cells (with the exclusion of staurosporine treatment). MFI values (Fig. 10H) were 2-fold higher in etoposide and staurosporine treated cells, suggesting, for the first treatment, an increase in the autophagy pattern able to maintain a good cell viability, whereas for the latter, an autophagic pattern as a cell death mechanism that can occur either in the absence of detectable signs of apoptosis (via autophagic cell death), or concomitantly with apoptosis.

Scatter and SYBR GREEN I evaluations

Propelled by TEM and CSLM observations, we labelled each sample by SYBR GREEN I (Fig. 11). This fluorochrome allowed us to distinguish differentiated cells with low and high green fluorescence (i.e with low and high DNA content.). The differences occurring in green fluorescence were also registered on myoblasts but with a different connotation: in fact, a low DNA content may also be related to apoptotic phenomena (dense heterochromatin and DNA cleavage) that were observed in the undifferentiated stage also linked to a certain shrinkage (low FSC and SSC values). On the other hand, in myotubes, cell death was negligible by both ultrastructural and cytometric evaluations and the decrease in SYBR GREEN I fluorescence was not accompanied by cell shrinkage. The Figure shows that higher percentages of these events (columns represent the lowest MFI green values) were found in etoposide and staurosporine-treated myotubes.

Discussion

In this study, the apoptotic behavior of myoblasts and myotubes has been compared after treatment with the same chemical agents, acting through DNA damage or oxidative stress and leading to a p53-dependent apoptotic death (Liu et al., 2011). The data obtained demonstrated a noteworthy apoptotic rate in skeletal muscle cells.

In particular, this work focused attention on myotube resistance to apoptosis as compared to myoblasts, evidenced using an ultrastructural approach and quantified by flow cytometric analyses. TEM revealed that chromatin condensation, a characteristic apoptotic feature more diffuse in myoblasts, appeared to be either organized in ring-shaped dense masses under the nuclear membrane, or uniformly condensed to occupy the entire nucleus. The well known cup-shaped chromatin patches, typical of classical programmed cell death, were not observed. Only in cells treated with staurosporine did a chromatin rearrangement, with an attempt at cup-shaped mass formation similar to that observed in U937 cells,

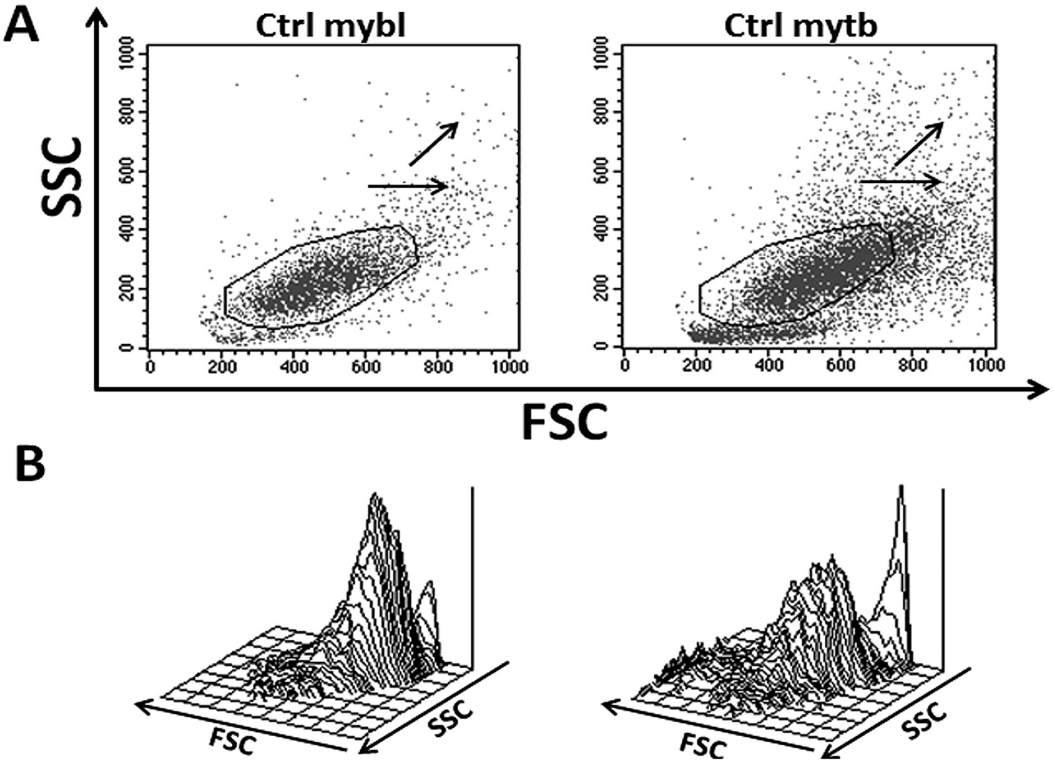

Fig. 7. Flow cytometric analyses of scatter characteristics of C2C12 myoblasts (ctrl mybl) and myotubes (ctrl mytb). Data are given as dot plot **(A)** and 3D isometric plot (**B**), to better visualize differences and homologies in these two samples. In **A**, arrows focus the peculiar changes in dot distribution along cellular differentiation, also appreciable in **B**.

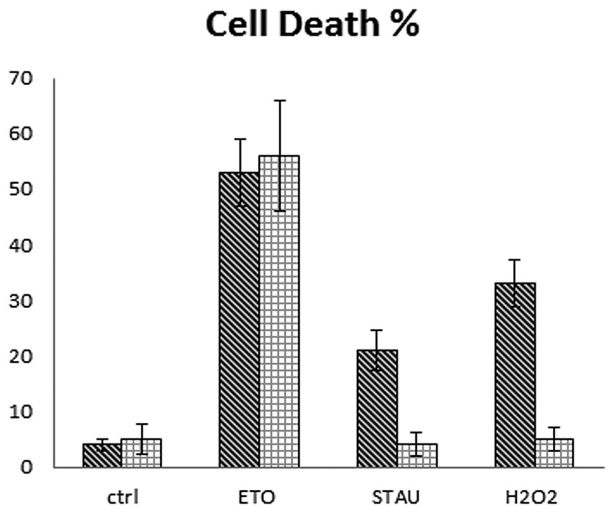

Fig. 8. Statistic histogram showing percentages of sub G1 events in each experimental condition. Data are from 3 separate experiments and are furnished as mean±SD. CTRL, control; ETO, etoposide; STAU, staurosporine; H_2O_2, hydrogen peroxide.

appear.

Thus in muscle cells, apoptotic nuclear changes, requiring lamin proteolysis and actin-myosin contractile force (Croft et al., 2005), appeared as a complex phenomenon.

This was also confirmed by the particular blebbing process that occurs with an early phase, characterized by cell retraction and small blebs formation - as observed in the present work - followed by a second phase, associated with large blebs, linked to chromatin splitting into apoptotic bodies (Cheng and Lane, 2010), typical of classical apoptosis.

Moreover, CLSM observations after the TUNEL reaction evidenced that DNA fragmentation occurred in muscle cells and was more evident in myoblasts compared to myotubes, as also confirmed by cytometric analysis of DNA content and of cardiolipin peroxidation. This myotube resistance to apoptosis could be explained considering firstly the cell phenotype: the mononucleated cells are more susceptible to stress signals than a multinucleated syncytium where each nucleus seems to have an independent domain (Alway and Siu, 2008). In this work, TEM and CLSM demonstrated that by exposing myotubes to etoposide

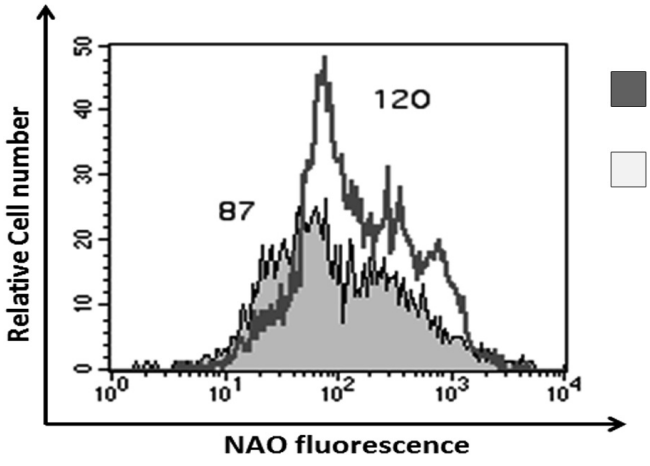

Fig. 9. Overlaid histograms related to NAO fluorescence intensity for control myoblasts (grey filled area) and control myotubes (deep grey line), illustrate higher IF values for myotubes, as expected by both literature data and typical mitochondria enrichment during differentiation. Changes in these steady-state values are given below, as statistic histogram. Statistic histogram related to NAO fluorescence detectionin myoblasts and myotubes, in control samples and after each treatment. Data are from 3 separate experiments and are furnished as mean±SD. The involvement of mitochondrial pathway in undifferentiated C2C12 cells and the absence of significant mitochondrial impairment in differentiated cells are evident.

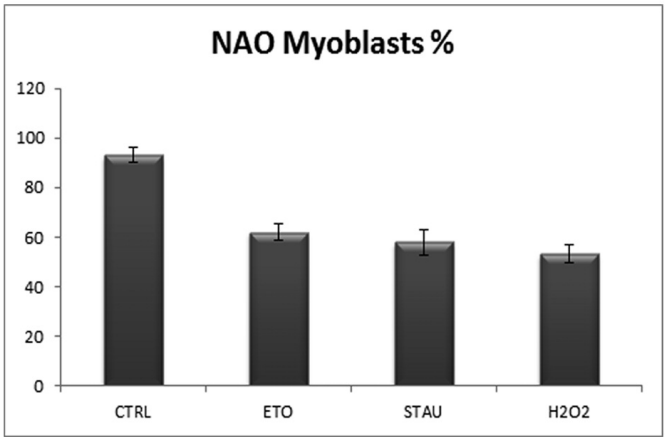

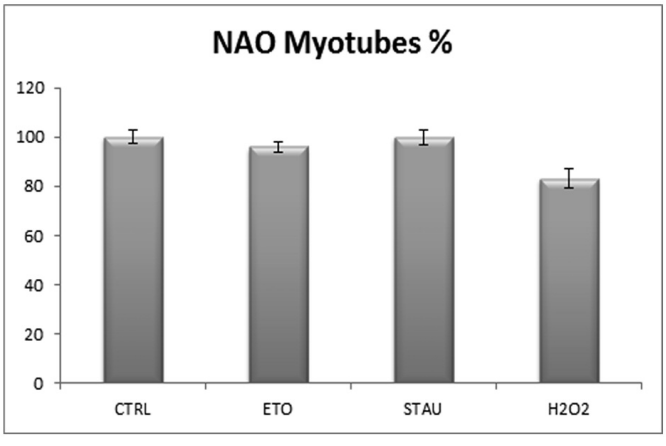

and staurosporine, apoptotic nuclei coexist with normal nuclei within the same fiber. Flow Cytometry by SYBR GREEN I detection distinguished cells with high nuclear content (HNC) and with low nuclear content (LNC). This finding may be correlated with previous observations. The high nucleic acid content of HNC cells can be explained in different ways. We may assume that LNC cells include an important fraction of dead cells, but this hypothesis is invalidated by all other tests. Therefore it is conceivable that LNC cells are those characterized by coexistence of apoptotic nuclei with normal nuclei within the same fiber. This confirms the

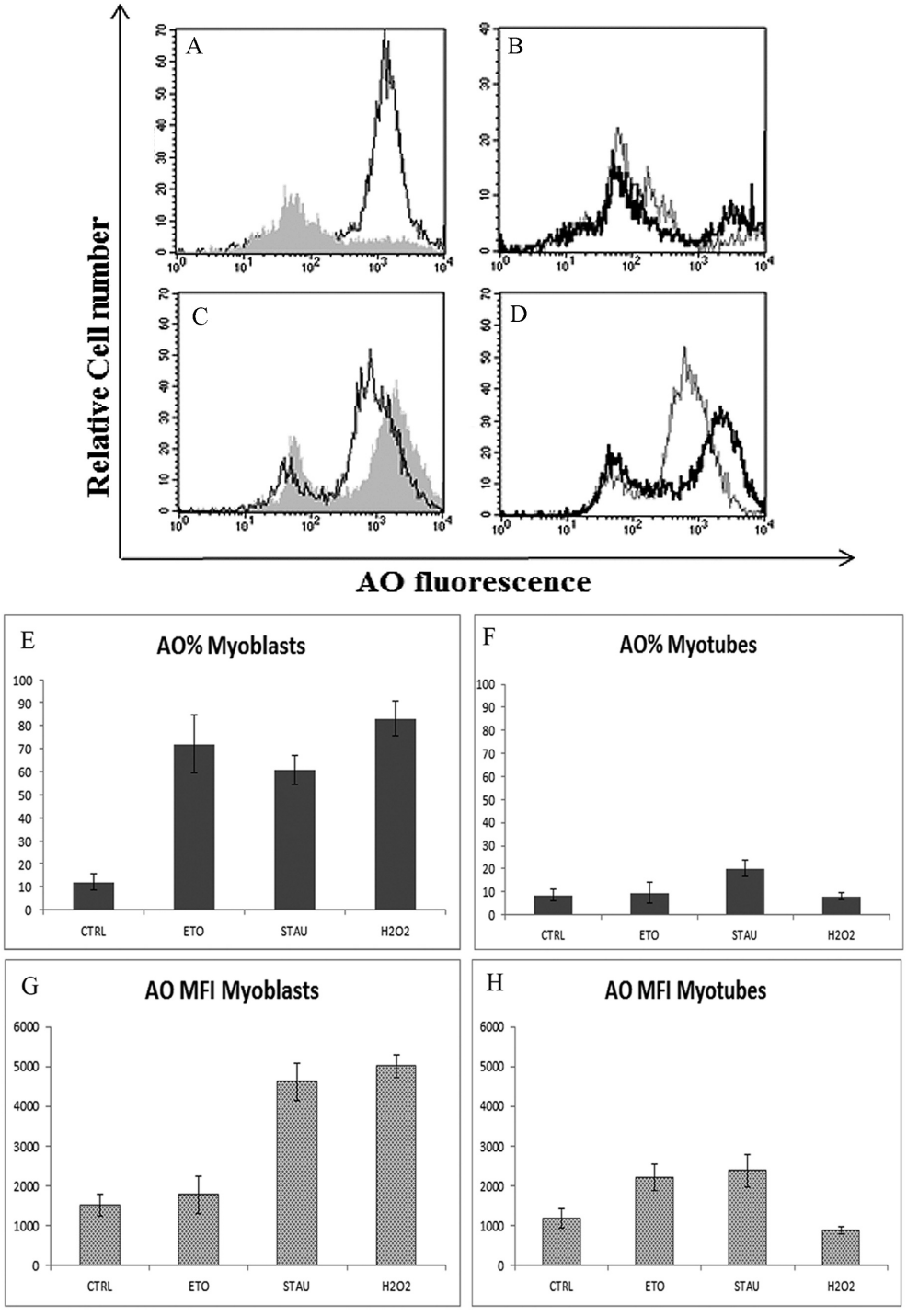

Fig. 10. Histograms related to AO fluorescence for Myoblasts **(A, B)** and Myotubes **(C, D)** for each experimental condition (overlaid). The black line is for control value **(A, C),** the filled light grey gaussian is for etoposide **(A, C)**, the bold black line is for staurosporine **(B, D)** and the grey line is for H_2O_2 **(B, D)** Statistic histograms related to percentages (AO%) of AO dim (cell population with low intensity fluorescence) events **(E, F)** and to AO MFI values of AO bright (cell population with high intensity fluorescence) events **(G, H)** in myoblasts **(E, G)** and myotubes **(F, H)**. Data are from 3 separate experiments and are furnished as mean±SD.

notion of a "nuclear apoptosis" working to selectively remove the designated myonuclei in the multinucleated syncytium (Siu and Alway, 2009; Marzetti et al., 2010). This phenomenon, even if still considered a controversial point (Bruusgaard and Gundersen, 2008), has been demonstrated in our previous work in UVB-treated myotubes (D'Emilio et al., 2010), and has been, recently, reported by other authors (Armand et al., 2011; Guo et al., 2012). Therefore, in mononucleated cells, apoptosis is responsible for nucleus deletion and later for the death of the entire cell (Alway and Siu, 2008), while in myotubes apoptosis is limited to one nuclear domain.

The deletion of a single nucleus could occur without the death of the entire muscle fiber at the same time, evidencing that a multinucleated cell dies "more slowly".

Moreover, TEM observations revealed a widespread presence of autophagic vacuoles, especially in myotubes. These organelles, absent in control myoblasts and myotubes, probably play a role in muscle fiber integrity maintenance, as reported by several authors (Masiero et al., 2009; Alger et al., 2011; Xiao et al., 2011). The presence of this mechanism in myotube response to apoptotic triggers can be considered another element involved in their resistance to apoptosis. In fact, TEM observations revealed that these organelles contain degenerated mitochondria, condensed chromatin, free ribosomes and membranes, suggesting that autophagy is important to preserve muscle mass, to maintain myofiber integrity, and to protect against cell damage.

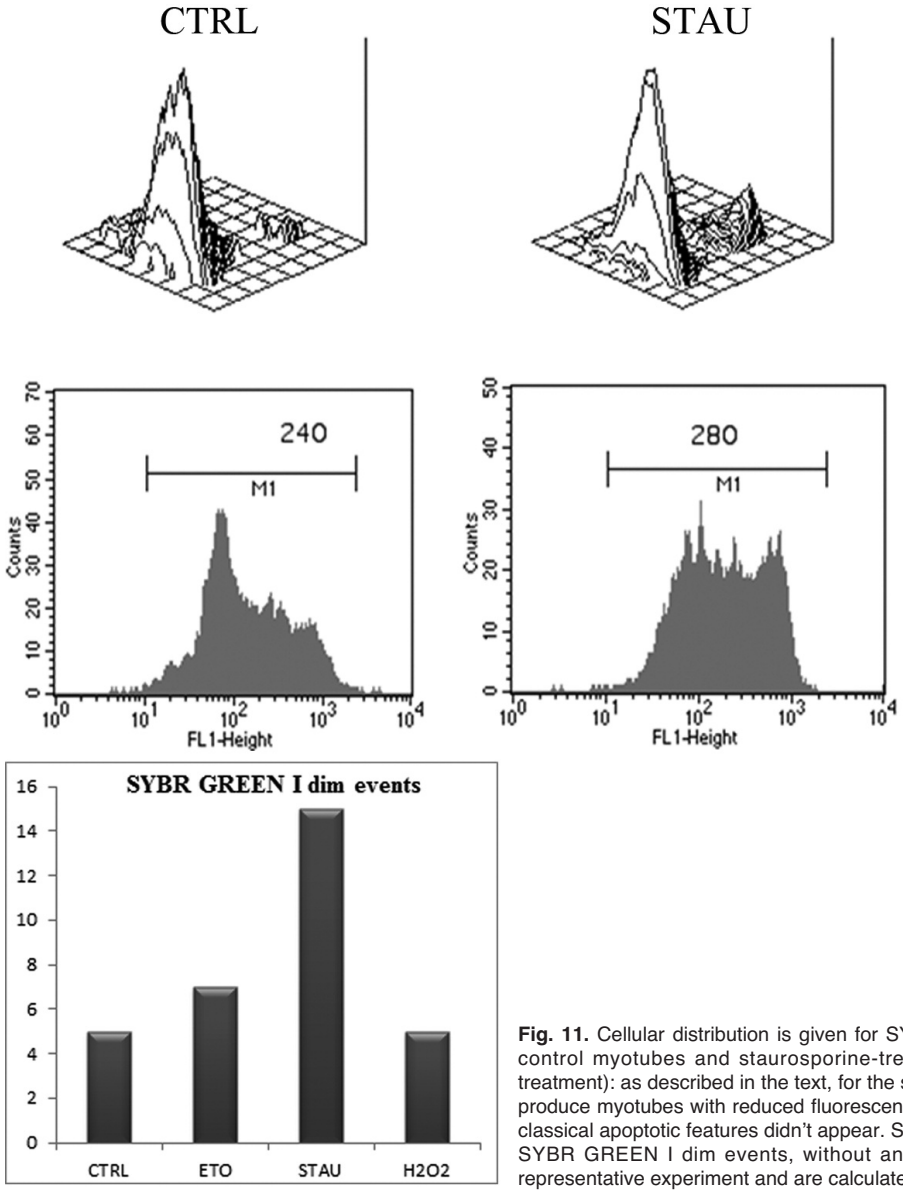

Fig. 11. Cellular distribution is given for SYBR GREEN I fluorescence and FSC, comparing control myotubes and staurosporine-treated myotubes (considered as representative treatment): as described in the text, for the selected events, staurosporine treatment seems to produce myotubes with reduced fluorescence intensity for SYBR GREEN I staining, although classical apoptotic features didn't appear. Statistic histogram related to cytometric detection of SYBR GREEN I dim events, without any cell shrinkage phenomena. Data are from a representative experiment and are calculated only on differentiated C2C12 cells.

Inhibition/alteration of autophagy can indeed contribute to myofiber degeneration and muscle weakness in disorders characterized by accumulation of these inclusions (Masiero et al., 2009). Other studies evidenced that apoptosis-induced myonuclear debris removal seems to involve both the ubiquitin-proteasome pathway and the autophagic process. The latter can be regarded as an important mechanism for mitochondria degradation (Wohlgemuth et al., 2010; Grumati et al., 2011; Rambold and Lippincott-Schwartz, 2011), which becomes crucial when mitochondria are damaged and dysfunctional. Mitochondria activity, analysed by means of flow cytometry, significantly decrease after all chemical treatments in myoblasts, whereas in myotubes, altered mitochondria appeared, especially after H2O2 exposure. Mitochondria are both generators of and targets for reactive species. Mitochondria generate ROS (reactive oxygen species) from a number of different redox centers in the respiratory chain and other metabolic pathways. Therefore oxidative stress is inseparably linked to mitochondria dysfunction. It seems that in a syncytium, cellular antioxidant capability appeared to be better preserved and capable of maintaining a correct ROS level. Furthermore, different authors (McMillin and Dowhan, 2002) have linked cardiolipin peroxidation with cytochrome c release and this may confirm apoptotic events observed by TEM and CLSM techniques.

In summary, these findings demonstrate a peculiar apoptotic behavior in muscle cells with a different sensitivity of myoblasts and myotubes to apoptotic triggers. Recent papers have shown that several genes and proteins are involved in the negative regulation of apoptosis and their expression in differentiated myotubes is indeed higher than in myoblasts, indicating that these molecules may be responsible for the apoptosis resistance of myotubes (Kamradat et al., 2002; Xiao et al., 2011).

Further studies are in progress to highlight skeletal muscle death mechanisms, in particular myonuclear apoptotic behavior in multinucleated syncytium. In this condition, the most similar to that of adult skeletal muscle, apoptosis plays a crucial role in a number of muscle disorders and its understanding represents a positive progression in the scenario of muscle pathology.

Acknowledgements. This work was supported by the University of Urbino and the Ministry of Education, University and Research (PRIN 2009). We would like to thank Dr. Davide Curzi, Mr. Oliviero Rusciadelli and Mr. Lorenzo Bedini for their skilful technical assistance.

References

Adhihetty P.J., O'Leary M.F.N. and Hood D.A. (2009). Mitochondria in Skeletal Muscle: Adaptable Rheostats of Apoptotic Susceptibility. Exerc. Sport Sci. Rev. 36, 116-121.

Alger H.M., Raben N., Pistilli E., Francia D., Rawat R., Getnet D., Ghimbovschi S., Chen Y.W., Lundberg I.E. and Nagaraju K. (2011). The role of tumor necrosis factor-·-related apoptosis-inducing ligand (TRAIL) in mediating autophagy in myositis skeletal muscle: A potential non-immune mechanism of muscle damage. Arthritis Rheum. 63, 3448-3457.

Alway S.E. and Siu P.M. (2008). Nuclear apoptosis contributes to sarcopenia. Exerc. Sport Sci. Rev. 36, 51-57.

Andrianjafiniony T., Dupré-Aucouturier S., Letexier D., Couchoux H. and Desplanches D. (2010). Oxidative stress, apoptosis, and proteolysis in skeletal muscle repair after unloading. Am. J. Physiol. Cell Physiol. 299, C307–C315.

Armand A.S., Laziz I., Djeghloul D., Lécolle S., Bertrand AT., Biondi O., De Windt L.J. and Chanoine C. (2011). Apoptosis-inducing factor regulates skeletal muscle progenitor cell number and muscle phenotype. PLoS One 6, e27283.

Bruusgaard J.C. and Gundersen K. (2008). In vivo time-lapse microscopy reveals no loss of murine myonuclei during weeks of muscle atrophy. J. Clin. Invest. 118, 1450-1457.

Burattini S., Ferri P., Battistelli M., D'Emilio A., Biagiotti L., Sestili P., Rocchi M.B. and Falcieri E. (2009). Apoptotic DNA fragmentation can be revealed in situ: an ultrastructural approach. Microsc. Res. Tech. 72, 913-923.

Canonico B., Betti M., Luchetti F., Battistelli M., Falcieri E., Ferri P., Zamai L., Barnett D. and Papa S. (2010). Flow cytometric profiles, biomolecular and morphological aspects of transfixed leukocytes and red cells. Cyto. B Clin. Cytom. 78, 267-278.

Chen L., Feng X.C., Lu F., Xu X.L., Zhou G.H., Li Q.Y. and Guo X.Y. (2011). Effects of camptothecin, etoposide and Ca^{2+} on caspase-3 activity and myofibrillar disruption of chicken during post-mortem ageing. Meat. Sci. 87, 165-174.

Cheng J.P. and Lane J.D. (2010). Organelle dynamics and membrane trafficking in apoptosis and autophagy. Histol. Histopathol. 25, 1457-1472.

Croft D.R., Coleman M.L., Li S., Robertson D., Sullivan T., Stewart C.L. and Olson M.F. (2005). Actin-myosin–based contraction is responsible for apoptotic nuclear disintegration. J. Cell Biol. 168, 245–255.

D'Emilio A., Biagiotti L., Burattini S., Battistelli M., Canonico B., Evangelisti C., Ferri P., Papa S., Martelli A.M. and Falcieri E. (2010). Morphological and biochemical patterns in skeletal muscle apoptosis. Histol. Histopathol. 25, 21-32.

Ferreira R., Neuparth M.J., Vitorino R., Appell H.J., Amado F. and Duarte J.A. (2008). Evidences of apoptosis during the early phases of soleus muscle atrophy in hind-limb suspended mice. Physiol. Res. 57, 601-611.

Ghosh D. and Barry M.A. (2005). Selection of muscle-binding peptides from context-specific peptide-presenting phage libraries for adenoviral vector targeting. J. Virol. 79, 13667-13672.

Govindaraju V., Michoud M.C, Al-Chalabi M., Ferraro P., Powell W.S and Martin J.G. (2006). Interleukin-8: novel roles in human airway smooth muscle cell contraction and migration. Am. J. Physiol. Cell Physiol. 291, C957-965.

Grumati P., Coletto L., Schiavinato A., Castagnaro S., Bertaggia E., Sandri M. and Bonaldo P. (2011). Physical exercise stimulates autophagy in normal skeletal muscles but is detrimental for collagen VI deficient muscles. Autophagy 7, 1415-1423.

Guo B.S., Cheung K.K., Yeung S.S., Zhang B.T. and Yeung E.W. (2012). Electrical stimulation influences satellite cell proliferation and apoptosis in unloading-induced muscle atrophy in mice. PLoS One 7, e30348.

Jeong S.Y. and Seol D.W. (2008). The role of mitochondria in apoptosis. BMB Rep. 41, 11–22.

Kamradt M.C., Chen F., Sam S. and Cryns V.L. (2002). The small heat shock protein alpha B-crystallin negatively regulates apoptosis during myogenic differentiation by inhibiting caspase-3 activation. J. Biol. Chem. 277, 38731-38736.

Lebaron P., Servais P., Agogué H., Courties C. and Joux F. (2001). Does the high nucleic acid content of individual bacterial cells allow us to discriminate between active cells and inactive cells in aquatic systems? Appl. Environ. Microbiol. 67, 1775-1782.

Liu J., Uematsu H., Tsuchida N. and Ikeda M.A. (2011). Essential role of caspase-8 in p53/p73-dependent apoptosis induced by etoposide in head and neck carcinoma cells. Mol. Cancer 31, 10-95

Luchetti F., Canonico B., Curci R., Battistelli M., Mannello F., Papa S., Tarzia G. and Falcieri E. (2006). Melatonin prevents apoptosis induced by UV-B treatment in U937 cell line. J. Pineal Res. 40, 158-167.

Luchetti F., Canonico B., Mannello F., Masoni C., D'Emilio A., Battistelli M., Papa S. and Falcieri E. (2007). Melatonin reduces early changes in intramitochondrial cardiolipin during apoptosis in U937 cell line. Toxicol. In Vitro 21, 293-301.

Marzetti E., Hwanga J.C.Y, Lees H.A., Wohlgemutha S.E., Dupont-Versteegdenc E.E., Cartera C.S., Bernabeib R. and Leeuwenburgha C. (2010). Mitochondrial death effectors: Relevance to sarcopenia and disuse muscle atrophy. Biochim. Biophys. Acta 1800, 235-244.

Masiero E., Agatea L., Mammucari C., Blaauw B., Loro E., Komatsu M., Metzger D., Reggiani C., Schiaffino S. and Sandri M. (2009). Autophagy is required to maintain muscle mass. Cell Metab. 10, 507-515.

McMillin J.B. and Dowhan W. (2002). Cardiolipin and apoptosis. Biochim. Biophys. Acta 1585, 97-107.

Munoz J., Zhou Y. and Jarrett H.W. (2010). LG4-5 domains of laminin-211 binds alpha-dystroglycan to allow myotube attachment and prevent anoikis. J. Cell Physiol. 222, 111-119.

Rambold A.S. and Lippincott-Schwartz J. (2011). Mechanisms of mitochondria and autophagy crosstalk. Cell Cycle 10, 4032-4038.

Salucci S., Battistelli M., Burattini S., Squillace C., Canonico B., Gobbi P., Papa S. and Falcieri E. (2010). C2C12 myoblast sensitivity to different apoptotic chemical triggers. Micron 41, 966-973.

Siu P.M. and Alway S.E. (2009). Response and adaptation of skeletal muscle to denervation stress: the role of apoptosis in muscle loss. Front. Biosci. 14, 432-452.

Siu P.M. (2009). Muscle apoptotic response to denervation, disuse, and aging. Med. Sci. Sports Exerc. 41, 1876-1886.

Traganos F. and Darzynkiewicz Z. (1994). Lysosomal proton pump activity: supravital cell staining with acridine orange differentiates leukocyte subpopulations. Methods Cell Biol. 41, 185-194.

Tews D.S. (2003). Role of apoptosis in myopathies. Basic Appl. Myol. 13, 181-190.

Wang J., Guo K., Wills K.N. and Walsh K. (1997). Rb functions to inhibit apoptosis during myocyte differentiation. Cancer Res. 57, 351-354.

Wei H., Li Z., Hu S., Chen X. and Cong X. (2010). Apoptosis of mesenchymal stem cells induced by hydrogen peroxide concerns both endoplasmic reticulum stress and mitochondrial death pathway through regulation of caspases, p38 and JNK. J. Cell Biochem. 111, 967-978.

Wohlgemuth S.E., Arnold Young Seo A.Y., Marzetti E., Lees H.A. and Leeuwenburgh C. (2010). Skeletal muscle autophagy and apoptosis during aging: effects of calorie restriction and life-long exercise. Exp. Gerontol. 45, 138-148.

Xiao R., Ferry A.L. and Dupont-Versteegden E.E. (2011). Cell death-resistance of differentiated myotubes is associated with enhanced anti-apoptotic mechanisms compared to myoblasts. Apoptosis 16, 221-234.

Zamai L., Burattini S., Luchetti F., Canonico B., Ferri P., Melloni E., Gonelli A., Guidotti L., Papa S. and Falcieri E. (2004). In vitro apoptotic cell death during erythroid differentiation. Apoptosis 9, 235-246.

Zhang Z.D. and Cox G. (1998). Use of flow cytometry to study growth of human airway smooth muscle cells. In Vitro Cell Dev. Biol. Anim. 34, 275-277.

Zhang R., Lee I.K., Piao M.J., Kim K.C., Kim A.D., Kim H.S., Chae S., Kim H.S. and Hyun JW. (2011). Butin (7,3',4'-Trihydroxydihydro-flavone) Reduces Oxidative Stress-Induced Cell Death via Inhibition of the Mitochondria-Dependent Apoptotic Pathway. Int. J. Mol. Sci. 12, 3871-3887.

Accepted February 12, 2013